Journal of Engineering and Technology for Industrial Applications

ITEGAM-JETIA

Manaus, v.11 n.56, p.366-374. November/December, 2025.
DOI: https://doi.org/10.5935/jetia. v11i56.2897

ISSN ONLINE: 2447-0228

RESEARCH ARTICLE OPEN ACCESS

ITERATIVE FEEDBACK–OPTIMIZED IHS PANSHARPENING: APPLICATION TO IKONOS IMAGERY

Ghadjati Mohamed[1], Bouchemel Ammar[2], Mehallel Elhadi[3] and Moussaoui Abdelkrim[4]

[1]Laboratoire de Génie Électrique de Guelma (LGEG), Department of Electronics and Telecommunications, Faculty of Science and Technology, Université 8 mai 1945, BP 401, Guelma 24000, Algeria.
[2]Advanced Control Laboratory (LABCAV), Department of Electronics and Telecommunications, Faculty of Science and Technology, Université 8 mai 1945, BP 401, Guelma 24000, Algeria.
[3]Laboratory of Telecommunication and Smart Systems (LTSS), Faculty of Science and Technology University of Djelfa, PO Box 3117, Djelfa 17000 Algeria.
[4]Laboratoire de Génie Électrique de Guelma (LGEG), Department of Automatic and Electrotechnical Engineering, Faculty of Science and Technology, Université 8 mai 1945, BP 401, Guelma 24000, Algeria.

[1]https://orcid.org/0000-0001-8298-5736, [2]https://orcid.org/0000-0002-2861-4819
[3]https://orcid.org/0000-0001-7488-162X, [4]https://orcid.org/0000-0002-8870-8809

Email: ghadjati.mohamed@univ-guelma.dz, bouchemel.ammar@univ-guelma.dz, e.mehallel@univ-djelfa.dz, moussaoui.abdelkrim@univ-guelma.dz

ARTICLE INFO

Article History
Received: November 6, 2025
Revised: November 20, 2025
Accepted: December 1, 2025
Published: December 31, 2025

Keywords:

Image fusion,
Pansharpening,
feedback optimization,
low-pass filtering,
QNR index.

ABSTRACT

Intensity-Hue-Saturation (IHS) is a component-substitution method that employs mathematical transformation between IHS and Red-Green-Blue (RGB) color domains to transfer spatial detail from the panchromatic image to the resampled multispectral bands. In this study, an iterative feedback-optimized approach is proposed to enhance the IHS pansharpening method. This approach starts by applying a low-pass filter to the output of the IHS fusion, resulting in an updated low-resolution multispectral image. This image is then reintroduced into the IHS fusion process, and the steps are repeated until a predefined quality threshold, measured by the Quality with No Reference (QNR) index, is achieved. The mathematical analysis demonstrates that this iterative approach transfers spatial details from the panchromatic image to the multispectral bands gradually over multiple iterations, in contrast to the standard IHS method where this detail injection occurs in a single step. This allows controlled and data-driven enhancement of spatial information. Experiments using IKONOS satellite images show that the proposed approach consistently improves the fusion quality of IHS pansharpening both numerically and visually, compared to the standard IHS algorithm and to two alternative baseline methods: Principal Component Analysis (PCA) and High-Pass Filtering (HPF).

I. INTRODUCTION

Pansharpening is an image fusion technique, operating at the pixel level, that combines the satellite multispectral (MS) and panchromatic (PAN) images to create a new multispectral image with the details of the PAN image. The importance of pansharpening comes from its power to create images that combine the spatial clarity of PAN images with the spectral richness of MS images, resulting in colored image with clearer objects which is crucial for accurate analysis and interpretation in various applications. These applications include environmental monitoring, urban planning, agriculture, and disaster management, where precise and detailed imagery is essential for making informed decisions and conducting comprehensive analyses.

There are many ways to categorize pansharpening methods. One simple classification by Schowengerdt [1] divides them into three categories: spectral domain techniques (like PCA and IHS) [2], spatial domain techniques (such as HPF and high–frequency modulation [3] and high frequency modulation (HFM) [1], and scale–space techniques (like wavelet–based methods). Amro et al. (2011) [4] categorize pansharpening methods into the following families: the component substitution (CS) family, which includes PCA, IHS, and Gram-Schmidt (GM) methods [5]; the relative spectral contribution (RSC) family, with methods like the Brovey transform (BT) [6]; the high–frequency injection family, including HPF and HFM methods; the multiresolution family, based on wavelet transforms, including Mallat's algorithm [7–11] and the 'à trous' algorithm (ATW) [12]; and fusion methods based on image statistics, like the Price method [13], [14]. Pohl and Van Genderen [15] proposed a recent classification of pansharpening methods into six main groups. The first is component substitution, including methods like IHS. The second is numerical methods, which use basic operations such as addition, subtraction, multiplication, and ratio between image bands. Brovey Transform (BT) is a popular example. The third is statistical fusion, using methods like principal component analysis (PCA). The fourth is multiresolution techniques, based on tools like the wavelet transform. The fifth group is hybrid methods, which combine two or more of the earlier approaches, such as Wavelet–PCA or Wavelet–IHS. Lastly, there are advanced methods, which go beyond traditional techniques. These include sparse representation and compressed sensing [16–19], Bayesian methods [20], and variational approaches [21]. For more details, see Alparone et al. [22]. In recent years, deep learning (DL) has played a key role in many research areas, thanks to advances in computer hardware and algorithms. The first use of DL in pansharpening dates back to 2015, with an autoencoder model introduced by Huang et al. [23]. Since then, several DL techniques have been applied to pansharpening, including convolutional neural networks (CNNs) [24–32], residual networks [33, 34], deep Laplacian pyramid networks (LapSRN) [35], [36], and generative adversarial networks (GANs) [37]. For more on machine learning in pansharpening, see Deng et al. [38]. This paper is divided into six sections. The next section gives a brief overview of the classical IHS fusion method. Section III introduces the proposed technique for improving the IHS pansharpening method. In section IV, a detailed mathematical modeling and analysis are presented in order to obtain a deep understanding of how the proposed techniqe works. In Section V, the enhancing method is tested and evaluated using IKONOS images, and the results are discussed both visually and with numerical measures. Finally, Section VI presents the conclusions and future directions.

II. IHS METHOD

Intensity-Hue-Saturation (IHS) transformation is a transformation between color spaces that converts a three-band image from the RGB (Red–Green–Blue) color space to the IHS (Intensity–Hue–Saturation) color space. Hence, it can be noticed that this method is limited to the fusion of images with only three spectral bands. The basic concept underlying this method is the capability of the IHS transformation to separate the spatial information into the intensity component (I). The mathematical model, along with various variants of this method, is presented in detail in [39]. Furthermore, the authors in [6] provided a generalized version of IHS method to images with more than three spectral bands, termed Generalized IHS (GIHS), where the Intensity component (I) is computed using the arithmetic mean across all bands. Hence, after stretching the PAN image to have the mean and variance of the intensity component, the fused image (HMS) is obtained through the diagram shown in the forward section of Figure 1, or equivalently by applying the following expression [40]:

$$\mathrm{HMS} = \mathrm{LMS} + \left(\mathrm{PAN} - I\right) \tag{1}$$

Where $I = \left(1/L\right)\sum_{l=1}^{L} \mathrm{LMS}_l$ is the intensity component, and LMS refers to the low-resolution multispectral image at the size of the PAN image (unlike the MS image of the original size before upsampling). Note that LMS is a multiband image, while PAN and I are single-band images. Therefore, the image (PAN – *I*) is added to each band of the LMS image.

III. PROPOSED TECHNIQUE FOR IMPROVING THE IHS METHOD

As shown in Figure 1, the proposed technique consists of two main sections: the forward section and the feedback section. The forward section implements the IHS method for image fusion. The feedback section applies low-pass filtering to the fused image and feeds it back into the process to iteratively enhance the fusion. This process is repeated until the optimal fused image is achieved, based on a selected quality assessment criterion. Moreover, we note that the quality assessment criterion used in this paper, denoted by Q in the figure, is the QNR index (Quality with No Reference) given by the following expression [41]:

$$QNR = \left(1 - D_{\lambda}\right)\left(1 - D_{S}\right) \tag{2}$$

Where D_λ and D_S represent the spectral distortion and spatial distortion indices, respectively, defined as follows:

$$D_{\lambda} = \sqrt{\frac{1}{L\left(L-1\right)}\sum_{l}^{L}\sum_{\substack{r=1 \\ r\neq l}}^{L}\left|Q\left(\mathrm{HMS}_l, \mathrm{HMS}_r\right) - Q\left(\mathrm{MS}_l, \mathrm{MS}_r\right)\right|} \tag{3}$$

$$D_{S} = \sqrt{\frac{1}{L}\sum_{l=1}^{L}\left|Q\left(\mathrm{HMS}_l, \mathrm{PAN}\right) - Q\left(\mathrm{MS}_l, \mathrm{PAN}^{lp}\right)\right|} \tag{4}$$

Where HMS refers to the fused image, MS to the original low-resolution multispectral image (i.e., with the original size), and PAN refers to the panchromatic image. The PAN^{lp} image is obtained by applying, to the panchromatic image, a lowpass filter with a normalized cutoff frequency at the resolution ratio, designed to match the Modulation Transfer Function (MTF) of the panchromatic sensor, followed by decimation. Note that, in Equations (2) and (3), *Q* denotes the *Q*–index defined in [42] as follows:

$$Q = \frac{\sigma_{xy}}{\sigma_x \sigma_y} \cdot \frac{2\bar{x}.\bar{y}}{(\bar{x})^2 + (\bar{y})^2} \cdot \frac{2\sigma_x \sigma_y}{\sigma_x^2 + \sigma_y^2} \tag{5}$$

Where $\bar{x}$ and $\bar{y}$ represent the arithmetic mean over the spectral bands of *x* and *y* images, given by:

$$\bar{x} = \frac{1}{L}\sum_{i=1}^{L} x_i \quad , \quad \bar{y} = \frac{1}{L}\sum_{i=1}^{L} y_i \tag{6}$$

The quantities σ_x^2 and σ_y^2 represent the variances of *x* and *y* images given by:

$$\sigma_x^2 = \frac{1}{L-1}\sum_{i=1}^{L}(x_i - \bar{x})^2 \quad , \quad \sigma_y^2 = \frac{1}{L-1}\sum_{i=1}^{L}(y_i - \bar{y})^2 \tag{7}$$

Furthermore, the covariance between the two images x and y is obtained using the following expression:

$$\sigma_{xy} = \frac{1}{L-1}\sum_{i=1}^{L}(x_i - \bar{x})(y_i - \bar{y}) \tag{8}$$

The dynamic range of Q-index is $[-1,1]$.

It is worth noting that the authors in [43], [44] have proposed techniques similar to our enhancement approach, referred to as IPCA and IIHS, respectively. However, the key difference between their methods and the one proposed in this work lies in how the high-frequency details from the PAN image are incorporated. In the IPCA and IIHS approaches, a high-pass filter is applied in the forward section to extract high-frequency components from the PAN image, which are then injected into the PC1 or I component. In contrast, our method replaces the entire component with the PAN image, resulting in a different fusion strategy. The following section provides the mathematical details of the IHS method combined with the proposed enhancement technique as illustrated in Figure 1. The final mathematical expression describing this process gives a clear interpretation of how the technique works.

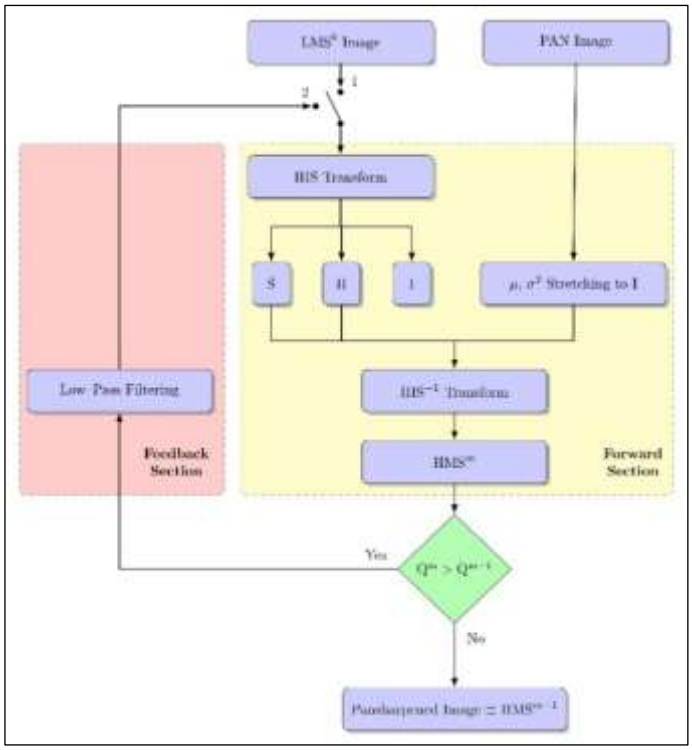

Figure 1: Block diagram of the proposed technique. The switch is initially set to position 1. Once the LMS^0 image is feeds the forward section, the switch changes to position 2.
Source: Authors, (2025).

IV. MODELING AND ANALYSIS OF THE PROPOSED ENHANCEMENT

The two fundamental equations governing the process shown in Figure 1 are given below. The first equation represents the forward process, while the second corresponds to the feedback process, both evaluated at the m–th iteration.

$$\mathrm{HMS}^m = \mathrm{LMS}^m + \left(\mathrm{PAN} - I^m\right) \tag{9}$$

$$\mathrm{LMS}^m = \mathrm{LPF}\left[\mathrm{HMS}^{m-1}\right] \tag{10}$$

Where $I^m = (1/L)\sum_{l=1}^{L} \mathrm{LMS}_l^m$ and $\mathrm{LPF}[\mathrm{g}]$ is the lowpass filter of the feedback section. HMS^m and LMS^m are the high–resolution and low–resolution images at iteration *m*, respectively. Note that for $m = 0$, Equation (9) corresponds to the classical IHS method.

To fairly compare the proposed enhancement method with the classical method, it is important to express the fused image at the *m*-th iteration, HMS^m, using only the available data: PAN, LMS^0, and I^0. Therefore, for $m = 1$, and using Equations (9) and (10) we obtain the following expression for the fused image:

$$\begin{aligned} \mathrm{HMS}^1 &= \mathrm{LMS}^1 + \left(\mathrm{PAN} - I^1\right) \\ &= \mathrm{LPF}\left[\mathrm{HMS}^0\right] + \left(\mathrm{PAN} - I^1\right) \\ &= \mathrm{LPF}\left[\mathrm{LMS}^0\right] + \mathrm{LPF}\left[\mathrm{PAN} - I^0\right] + \left(\mathrm{PAN} - I^1\right) \end{aligned} \tag{11}$$

By following the same reasoning, the general expression at the *m*-th iteration is given as:

$$\mathrm{HMS}^m = \mathrm{LPF}^m\left[\mathrm{LMS}^0\right] + \sum_{i=0}^{m} \mathrm{LPF}^i\left[\mathrm{PAN} - I^{m-i}\right] \tag{12}$$

Let $\mathrm{ARM}[\mathrm{g}] = (1/L)\sum_{l=1}^{L}(\mathrm{g})_l$ be the arithmetic mean across the *L* bands of the multispectral image. Furthermore, note that the lowpass filtering and arithmetic mean are interchangeable i.e., $\mathrm{ARM}\left[\mathrm{LPF}(\mathrm{g})\right] = \mathrm{LPF}\left[\mathrm{ARM}(\mathrm{g})\right]$. The intensity component at the *m*-th iteration, I^m, can be substituted as follows:

$$\begin{aligned} I^m &= \mathrm{ARM}\left[\mathrm{LMS}^m\right] \\ &= \mathrm{ARM}\left[\mathrm{LPF}\left[\mathrm{HMS}^{m-1}\right]\right] \\ &= \mathrm{ARM}\left[\mathrm{LPF}\left[\mathrm{LMS}^{m-1} + \left(\mathrm{PAN} - I^{m-1}\right)\right]\right] \\ &= \mathrm{LPF}\left[\mathrm{ARM}\left[\mathrm{LMS}^{m-1}\right]\right] + \mathrm{LPF}[\mathrm{PAN}] - \mathrm{LPF}\left[I^{m-1}\right] \\ &= \mathrm{LPF}\left[I^{m-1}\right] + \mathrm{LPF}[\mathrm{PAN}] - \mathrm{LPF}\left[I^{m-1}\right] \\ &= \mathrm{LPF}[\mathrm{PAN}] \end{aligned} \tag{13}$$

Hence, the intensity component, I^m, is given by:

$$I^m = \begin{cases} I^0 & \text{if } m = 0 \\ \mathrm{LPF}[\mathrm{PAN}] & \text{if } m \neq 0 \end{cases} \tag{14}$$

By substituting Equation (14) into Equation (12), we obtain:

$$\begin{aligned} \mathrm{HMS}^m = {} & \mathrm{LPF}^m\left[\mathrm{LMS}^0\right] + \mathrm{LPF}^m\left[\mathrm{PAN} - I^0\right] + \\ & \sum_{i=0}^{m-1} \mathrm{LPF}^i\left[\mathrm{PAN} - \mathrm{LPF}[\mathrm{PAN}]\right] \end{aligned} \tag{15}$$

This can also be written as:

$$\mathrm{HMS}^m = \mathrm{LPF}^m\left[\mathrm{LMS}^0\right] + \sum_{i=0}^{m} \mathrm{LPF}^i\left[\mathrm{PAN} - \mathrm{PAN}^{lp}\right] \tag{16}$$

Where PAN^{lp} is given by:

$$\mathrm{PAN}^{lp} = \begin{cases} I^0 & \text{if } i = m \\ \mathrm{LPF}[\mathrm{PAN}] & \text{if } i = 0,\mathrm{L}\ ,m-1 \end{cases} \tag{17}$$

Where LPF^m represent the m times convolution of the lowpass filter at the feedback section i.e., $\mathrm{LPF}^m = \mathrm{LPF} * \mathrm{L} * \mathrm{LPF}$. Figure 2 shows the frequency response of LPF, LPF^2, LPF^3 and LPF^4, where the lowpass filter used is the 3×3 boxcar filter.

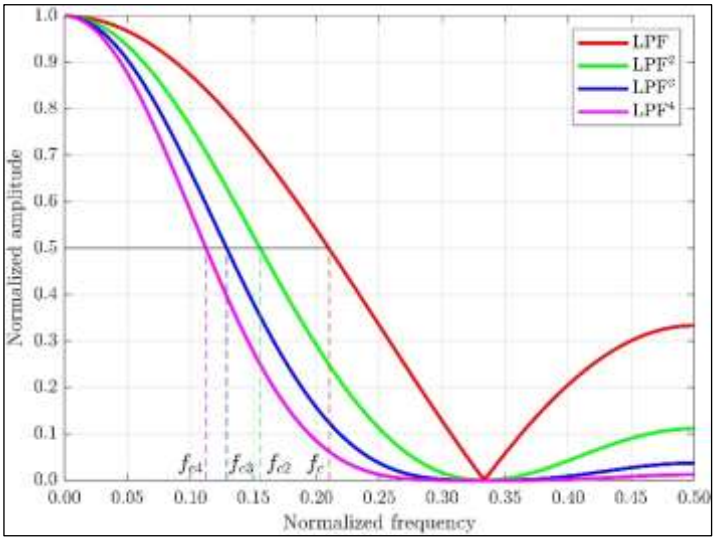

Figure 2: Frequency responses of LPF, LPF^2, LPF^3 and LPF^4 (LPF is 3×3 boxcar low-pass filter).
Source: Authors, (2025).

The right–hand side of Equation (16) comprises two terms: the first term represents the low frequency components contributed from the low–resolution multispectral image, LMS, while the second term represents the high–frequency components, or details, contributed from the high–resolution panchromatic image PAN. A closer examination of this equation reveals that the low–frequency components of the LMS image are extracted using a low–pass filter whose cutoff frequency depends on the iteration number *m*. As a result, the amount of retained low–frequency information varies across iterations, unlike in classical methods where it remains stable. On the other hand, the details are obtained through a discrete sum of high frequency contents extracted from the PAN image, also depending on the iteration number *m*. Furthermore, one can note that as *m* increases, the contribution of low-frequency components from the LMS image decreases, while the contribution of high-frequency details from the PAN image increases, and vice versa. In essence, the iteration number *m* serves as a control parameter that adjusts the balance between LMS and PAN content in the fused image. Hence, it can be concluded that each value of the iteration number *m* results in a distinct combination of low- and high-frequency content contributed by the LMS and PAN images, respectively, to form the fused image. This includes the combination corresponding to the classical method. However, as will be demonstrated experimentally later in this work, it is more likely that an alternative combination—different from the classical one—achieves superior fusion quality. This adaptive selection of the optimal fusion configuration represents the key novelty of the proposed enhanced technique.

V. EXPERIMENTAL RESULTS AND DISCUSSIONS

In this section, we conduct a comprehensive evaluation and comparison of the proposed enhanced technique, using both numerical and visual analyses. In the following subsection, we provide a brief overview of the study area used for the experiments.

V.1 STUDY AREA

To experimentally validate the proposed technique, we utilized two datasets acquired by the IKONOS sensors [45]. The 0.82–meter resolution panchromatic band (526–929 nm) was used in conjunction with four multispectral bands –blue (445–516 nm), green (506–595 nm), red (632–698 nm), and NIR (757–853 nm) – each with a spatial resolution of 3.28–meters. The radiometric resolution of these bands is 11 bits. The multispectral bands, originally sized at 100×200 pixels, was upsampled to 400×800 pixels using bicubic interpolation to match the size of the panchromatic band. The study area represents a densely populated urban environment characterized by a diverse array of high-frequency components including buildings, highways, lawns, trees, river, and bare soil. The scenes, raw data as well as fusion results, are shown in are shown in Figure 3.

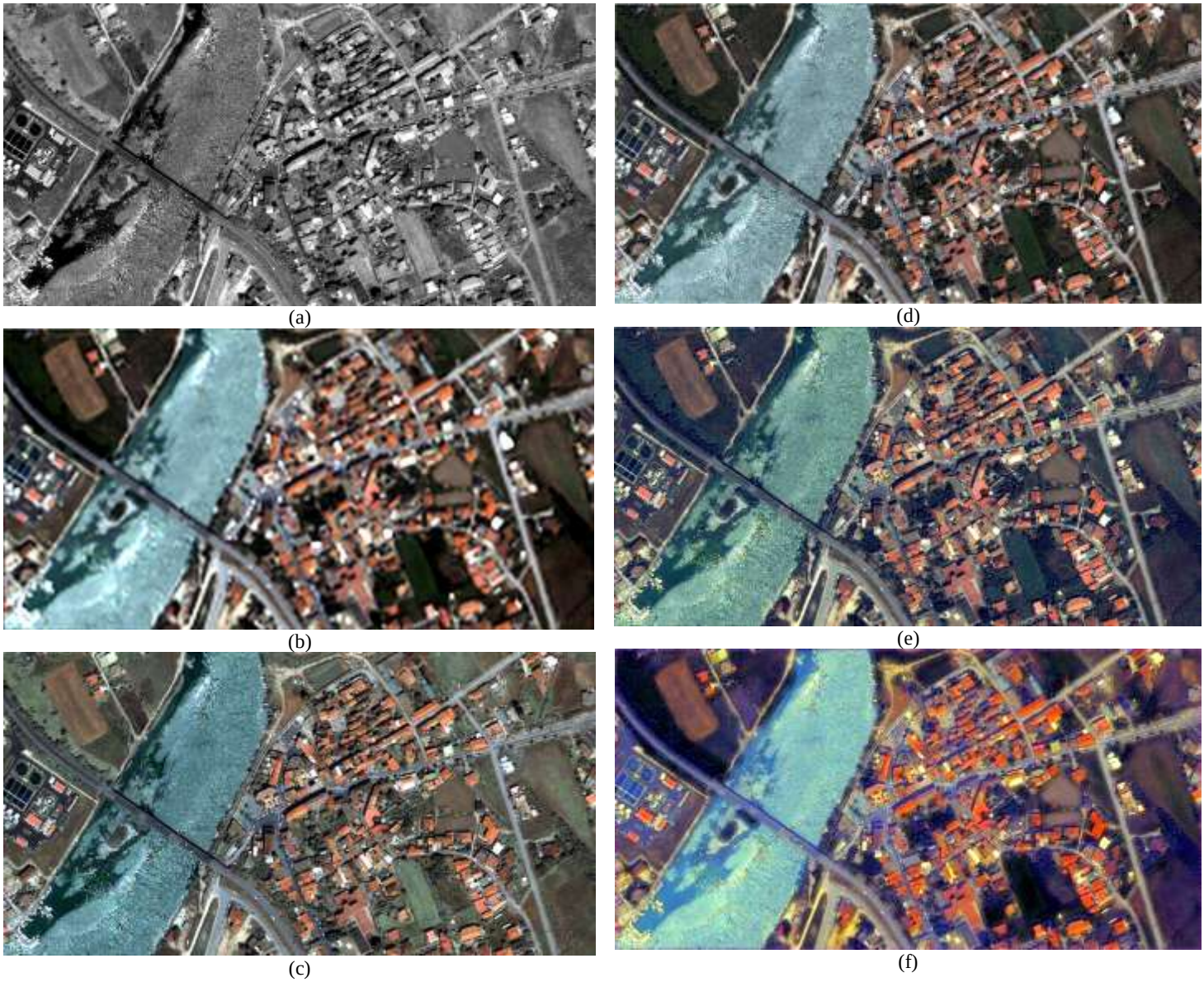

(a) (d) (b) (e) (c) (f)

Figure 3: IKONOS imagery raw data: (a) Pan, (b) LMS, and fusion results: (c) PCA, (d) HPF, (e) IHS, (f) IHS4.

V.2 QUALITATIVE ASSESSMENT

In this subsection, we visually examine the fused images based on two evaluation criteria: spatial detail enhancement and spectral information preservation. Specifically, we perform a visual comparison to assess how well the proposed technique incorporates spatial details from the PAN image while preserving spectral information from the LMS image. For spatial detail enhancement, the fused image is assessed to verify how well fine details, edges, and textures are captured compared to the original MS and PAN images. For spectral information preservation, we compare the color and spectral characteristics of the fused image with the original MS image. Note that, an effective pansharpening method maintains the original spectral information without introducing distortions or artifacts such as ringing around edges, color bleeding, or unnatural textures. Subsets from the PAN, LMS, and fused images using PCA, HPF, IHS, and the enhanced IHS with four iterations (i.e., for m=4, denoted as IHS4), are depicted in Figure 4, respectively. This subset includes various features such as trees, bare soil, and buildings, along with numerous textures and edges, making it both spectrally and spatially representative.

Visual inspection of the fusion results in Figure 3 and the corresponding subsets in Figure 4 shows a clear gain in terms of spatial detail of the fused images compared with the LMS image. Methods built on the enhancing framework outperform the classical pansharpening approaches, as clearly shown in Figure 3f. This observation agrees with the quantitative scores, which also indicate superior spatial quality for the enhancing framework across other conventional methods. The spatial gain, however, comes with an introduced color shifts or visible artifacts, as seen in the subsets of Figure 4. For example, PCA (Figure 4c) exhibits a noticeable green bias over grass and trees—especially clear in the north east corner of the fusion image—relative to the LMS reference (Figure 4b). HPF (Figure 4d) shows smaller chromatic deviations. The IHS result (Figure 4e) loses some color naturalness, with bluish/purplish tints that do not match the LMS image; this effect is stronger with IHS4 (Figure 4f), where the blue band, and to a lesser extent the red band, becomes dominant. Overall, the enhancing framework offers a consistent advantage in spatial quality on IKONOS data, while the remaining color deviations are moderate and, for many applications, an acceptable trade off.

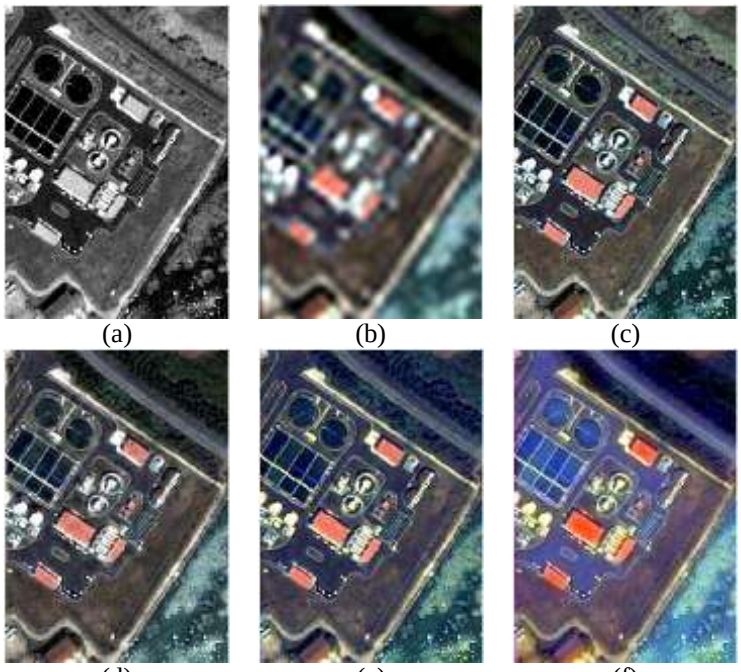

Figure 4: Subsets for qualitative assessment: (a) PAN image, (b) MS image, (c) PCA image, (d) HPF image, (e) IHS image (f) IHS4 image.
Source: Authors, (2025).

To further evaluate the effectiveness of the proposed enhancement framework, the next section presents quantitative metrics to complement the qualitative assessments discussed in the present subsection, resulting in a more comprehensive evaluation.

V.3 QUANTITATIVE ASSESSMENT

Table 1 lists the spectral distortion index D_λ, the spatial distortion index D_S, and the QNR index values for the different pansharpening methods. The best value for each index is emphasized in bold. The best results were observed with the enhanced IHS method after for iterations, referred to as IHS4, across all evaluation indices. A detailed analysis of the numerical results highlights the significant improvement achieved by the proposed technique, not only over the traditional IHS method but also over the PCA and HPF methods, both in terms of spatial and spectral quality. As shown in Table 1, the spectral distortion index of the IHS4 method is 0.031908, compared to 0.099749, 0.14856, and 0.13806 for the PCA, HPF, and IHS methods, respectively. This reflects a clear advantage in favor of the proposed enhancing framework. In terms of the spatial distortion index, the values are 0.065349 (IHS4), 0.23404 (PCA), 0.21534 (HPF), and 0.22012 (IHS). These results underline the superiority of the proposed method where the differences are several times larger over conventional methods. Similarly, the QNR index improves significantly from 0.67221 with the classical IHS method to 0.90483 with the proposed enhancement technique (IHS4), representing a substantial gain. It is also worth noting that the QNR values confirm the dominance of the enhanced IHS method over both the HPF method, which yields the lowest value, and the PCA method. In summary, the results of the three classical methods are close to each other yet markedly inferior to those of the enhancing framework for spectral, spatial, and QNR measures. Taken together, the visual assessment and quantitative results validate the theoretical analysis, confirming that the optimal fusion is not achieved through classical methods but rather through the proposed enhancement technique.

Table 1: Spectral, spatial and QNR indices for different fusion methods.

Method	D_λ	D_S	*QNR*
PCA	0.099749	0.23404	0.68955
HPF	0.14856	0.21534	0.66809
IHS	0.13806	0.22012	0.67221
IHS2	0.094735	0.15258	0.76714
IHS3	0.055919	0.08343	0.86532
IHS4	**0.031908**	**0.065349**	**0.90483**
IHS5	0.047142	0.075256	0.88115
IHS6	0.069136	0.11447	0.82431
IHS7	0.096651	0.15648	0.76199
IHS8	0.11664	0.18781	0.71746

Source: Authors, (2025).

VI. CONCLUSION AND FUTURE RESEARCH DIRECTIONS

This paper addresses the problem of image pansharpening, which aims to improve the spatial resolution of multispectral (MS) images by injecting high-frequency details from the panchromatic (PAN) image, while preserving the color (spectral) fidelity of the MS

data. Traditional pansharpening methods typically perform this detail injection as a fixed quantity through a single direct operation, based on the resolution ratio between PAN and MS images. However, this fixed quantity is not necessarily optimal in terms of either numerical or visual quality, as demonstrated by experimental results. To address this limitation, we proposed in this paper an enhancement for the IHS method based on iterative feedback optimization. In the proposed approach, the detail transfer from PAN to MS is performed in a closed-loop process, where each iteration produces a different combination of low-frequency components from the MS image and high-frequency details from the PAN image. This iterative process is guided by a fusion quality metric that terminates the iterations when further updates no longer improve the result. The key novelty of our method lies in its adaptive selection of the optimal frequency combination, which significantly improves fusion quality. When compared to benchmark methods such as IHS, PCA, and HPF, our approach demonstrates clear advantages and significant improvements both numerically and visually. Furthermore, this iterative optimization framework can be readily extended to other fusion techniques like PCA and HPF, maintaining the same principle of adaptive enhancement, while potentially yielding better results than their classical counterparts.

VII. AUTHOR'S CONTRIBUTION

Conceptualization: Ghadjati Mohamed.
Methodology: Ghadjati Mohamed.
Investigation: Ghadjati Mohamed,
Discussion of results: Ghadjati Mohamed, Ammar Bouchemel, Mehallel Elhadi.
Writing – Original Draft: Ghadjati Mohamed, Ammar Bouchemel, Mehallel Elhadi.
Writing – Review and Editing: Ghadjati Mohamed, Ammar Bouchemel, Mehallel Elhadi.
Resources: Ghadjati Mohamed, Moussaoui Abdelkrim.
Supervision: Moussaoui Abdelkrim.
Approval of the final text: Ghadjati Mohamed, Ammar Bouchemel, Mehallel Elhadi, Moussaoui Abdelkrim.

VIII. REFERENCES

[1] R. A. Schowengerdt, Remote Sensing: Models and Methods for Image Processing, 3rd ed., Academic Press, 2006.

[2] P. S. Chavez, S. C. Sides, and J. A. Anderson, "Comparison of three different methods to merge multiresolution and multispectral data: Landsat TM and SPOT panchromatic," Photogrammetric Engineering and Remote Sensing, vol. 57, no. 3, pp. 295–303, 1991.

[3] R. A. Schowengerdt, "Reconstruction of multispatial, multispectral image data using spatial frequency content," Photogrammetric Engineering and Remote Sensing, vol. 46, no. 10, pp. 1325–1334, 1980.

[4] I. Amro, J. Mateos, M. Vega, R. Molina, and A. K. Katsaggelos, "A survey of classical methods and new trends in pansharpening of multispectral images," EURASIP Journal on Advances in Signal Processing, 79 (2011). 2011.

[5] C. A. Laben, V. Bernard, and W. Brower, "Process for enhancing the spatial resolution of multispectral imagery using pan-sharpening," U.S. Patent. US & International, http://www.google.com/patents/US6011875, 2000.

[6] T. M. Tu, S. C. Su, H. C. Shyu, and P. S. Huang, "A new look at HIS-like image fusion methods," Information Fusion, vol. 2, no. 3, pp. 177–186, 2001.

[7] T. Ranchin, L. Wald, and M. Mangolini, "Efficient data fusion using wavelet transform: the case of SPOT satellite images," Proceedings Volume 2034, Mathematical Imaging: Wavelet Applications in Signal and Image Processing, 1993, pp. 171–178. DOI: 10.1117/12.147643.

[8] D. A. Yocky, "Image merging and data fusion by means of the discrete two-dimensional wavelet transform," Journal of the Optical Society of America, vol. 12, no. 9, pp. 1834–1841, 1995.

[9] B. Garguet-Duport, J. Girel, J. M. Chasseny, and G. Pautou, "The use of multiresolution analysis and wavelets transform for merging SPOT panchromatic and multispectral image data," Photogrammetric Engineering and Remote Sensing, vol. 62, no. 9, pp. 1057–1066, 1996.

[10] J. Zhou, D. L. Civco, and J. A. Silander, "A wavelet transform method to merge Landsat TM and SPOT panchromatic data," International Journal of Remote Sensing, vol. 19, no. 4, pp. 743–757, 1998.

[11] T. Ranchin, and L. Wald, "Fusion of high spatial and spectral resolution images: the ARSIS concept and its implementation," Photogrammetric Engineering and Remote Sensing, vol. 66, no.1, pp. 49–61, 2000.

[12] J. Núñez, X. Otazu, O. Fors, A. Prades, V. Palà, and R. Arbiol, "Multiresolution-based image fusion with additive wavelet decomposition," IEEE Transactions on Geoscience and Remote Sensing, vol. 37, no. 3, pp. 1204–1211, 1999.

[13] J. C. Price, "Combining panchromatic and multispectral imagery from dual resolution satellite instruments," Remote Sensing of Environment, vol. 21, no. 2, pp. 119–128, 1987.

[14] J. C. Price, "Combining multispectral data of differing spatial resolution," IEEE Transactions on Geoscience and Remote Sensing, vol. 37, no. 3, pp. 1199–1203, 1999.

[15] C. Pohl and J. Van Genderen, Remote Sensing Image Fusion: A Practical guide, CRC Press, 2017.

[16] S. Li, and B. Yang, "A new pan-sharpening method using a compressed sensing technique," IEEE Transactions on Geoscience and Remote Sensing, vol. 49, no. 2, pp. 738–746, 2011.

[17] S. Li, H. Yin, and L. Fang, "Remote sensing image fusion via sparse representations over learned dictionaries," IEEE Transactions on Geoscience and Remote Sensing, vol. 51, no. 9, pp. 4779–4789, 2013.

[18] X. X. Zhu, and R. Bamler, "A sparse image fusion algorithm with application to pansharpening," IEEE Transactions on Geoscience and Remote Sensing, vol. 51, no. 5, pp. 2827–2836, 2013.

[19] M. Cheng, C. Wang, and J. Li. “Sparse representation based pansharpening using trained dictionary,” IEEE Geoscience and Remote Sensing Letters, vol. 11, no. 1, pp. 293–297, 2014.

[20] Y. Zhang, S. De Backer, and P. Scheunders, “Noise-resistant wavelet-based Bayesian fusion of multispectral and hyperspectral images,” IEEE Transactions on Geoscience and Remote Sensing. vol. 47, no. 11, pp. 3834–3843, 2009.

[21] F. Palsson, J. R. Sveinsson, and M. O. Ulfarsson, “A new pansharpening algorithm based on total variation,” IEEE Geoscience and Remote Sensing Letters, vol. 11, no. 1, pp. 318–322, 2014.

[22] L. Alparone, B. Aiazzi, S. Baronti and A. Garzelli, Remote Sensing Image Fusion, CRC Press, 2015.

[23] W. Huang, L. Xiao, Z. Wei, H. Liu, and S. Tang, “A new pansharpening method with deep neural networks,” IEEE Geoscience and Remote Sensing Letters, vol. 12, no. 5, pp. 1037–1041, 2015.

[24] G. Masi, D. Cozzolino, L. Verdoliva, and G. Scarpa, “Pansharpening by convolutional neural networks,” Remote Sensing, vol. 8, no. 7, pp. 594, 2016.

[25] J. Zhong, B. Yang, G. Huang, F. Zhong, and Z. Chen, “Remote sensing image fusion with convolutional neural network,” Sensing and Imaging, vol. 17, no. 1, pp. 1–16, 2016.

[26] Y. Rao, L. He, and J. Zhu, “A residual convolutional neural network for pansharpening,” Proceedings the International Workshop on Remote Sensing with Intelligent Processing (RSIP), 18–21 May 2017, Shanghai, China, pp. 1–4 DOI: 10.1109/RSIP.2017.7958807.

[27] J. Yang, X. Fu, Y. Hu, Y. Huang, and J. Paisley, “PanNet: A deep network architecture for pan-sharpening,” Proceedings the IEEE International Conference on Computer Vision (ICCV), 22–29 October 2017, Venice, Italy, pp. 1753–1761. DOI: 10.1109/ICCV.2017.193.

[28] G. Scarpa, S. Vitale, and D. Cozzolino, “Target-adaptive CNN-based pansharpening,” IEEE Transactions on Geoscience and Remote Sensing, vol. 56, no. 9, pp. 5443–5457, 2018.

[29] Q. Yuan, Y. Wei, X. Meng, H. Shen, and L. Zhang, “A multiscale and multidepth convolutional neural network for remote sensing imagery pan-sharpening,” IEEE Journal of Selected Topics in Applied Earth Observations and Remote Sensing, vol. 11, no. 3, pp. 978–989, 2018.

[30] Z. Shao, and J. Cai, “Remote sensing image fusion with deep convolutional neural network,” IEEE Journal of Selected Topics in Applied Earth Observations and Remote Sensing, vol. 11, no. 5, pp. 1656–1669, 2018.

[31] W. Yao, Z. Zeng, C. Lian, and H. Tang, “Pixel-wise regression using U-Net and its application on pansharpening,” Neurocomputing, vol. 312, pp. 364–371, 2018.

[32] H. Zhang, and J. Ma. “GTP-PNet: A residual learning network based on gradient transformation prior for pansharpening,” ISPRS Journal of Photogrammetry and Remote Sensing, vol. 172, pp. 223–239, 2021.

[33] Y. Wei, Q. Yuan, H. Shen, and L. Zhang, “Boosting the accuracy of multispectral image pansharpening by learning a deep residual network,” IEEE Geoscience and Remote Sensing Letters, vol. 14, no. 10, pp. 1795–1799, 2017.

[34] J. Liu, Y. Feng, C. Zhou, and C. Zhang. “PWNet: An adaptive weight network for the fusion of panchromatic and multispectral images,” Remote Sensing, vol. 12, no, 17, pp. 2804, 2020.

[35] Y. Zhang, C. Liu, M. Sun, and Y. Ou, “Pan-sharpening using an efficient bidirectional pyramid network,” IEEE Transactions on Geoscience and Remote Sensing, vol. 57, no. 8, pp. 5549–5563, 2019.

[36] K. Li, W. Xie, Q. Du, and Y. Li, “DDLPS: Detail-based deep Laplacian pansharpening for hyperspectral imagery,” IEEE Transactions on Geoscience and Remote Sensing, vol. 57, no. 10, pp. 8011–8025, 2019.

[37] X. Liu, Y. Wang, and Q. Liu, “PSGAN: A generative adversarial network for remote sensing image pan-sharpening,” Proceedings the 25th IEEE International Conference on Image Processing (ICIP), 07–10 October 2018, Athens, Greece, pp. 873–877. DOI: 10.1109/ICIP.2018.8451049.

[38] L. -J. Deng, G. Vivone, M. E. Paoletti, G. Scarpa, J. He, Y. Zhang, J. Chanussot, and A. Plaza, “Machine Learning in Pansharpening A benchmark, from shallow to deep networks,” IEEE Geoscience and Remote Sensing Magazine, vol.10, no. 3, pp. 279–315, 2022.

[39] E. M. Schetselaar, “Fusion by the IHS transform: Should we use cylindrical or spherical coordinates?” International Journal of Remote Sensing, vol. 19, no. 4, pp. 759–765, 1998.

[40] Z. Wang, D. Ziou, C. Armenakis, D. Li, and Q. Li, “A comparative analysis of image fusion methods,” IEEE Transactions on Geoscience and Remote Sensing, vol. 43, no. 6, pp. 1391–1402, 2005.

[41] L. Alparone, B. Aiazzi, S. Baronti, A. Garzelli, F. Nencini, and M. Selva, “Multispectral and Panchromatic Data Fusion Assessment without Reference,” Photogrammetric Engineering and Remote Sensing, vol. 74, no. 2, pp. 193–200, 2008.

[42] Z. Wang, and A. C. Bovik, “A universal image quality index,” IEEE Signal Processing Letters, vol. 9, no. 3, pp. 81–84, 2002.

[43] M. Ghadjati, A. Moussaoui, and A. Boukharouba, “A novel iterative PCA-based pansharpening method,” Remote Sensing Letters, vol. 10, no. 3, pp. 264–273, 2019.

[44] M. Ghadjati, A. Benazza-Benyahia, A. Moussaoui, “Satellite Image Fusion Using an Iterative IHS-Based Approach,” Proceedings Mediterranean and Middle-East Geoscience and Remote Sensing Symposium (M2GARSS), 09–11 March 2020, Tunis, Tunisia, pp. 133–136. DOI: 10.1109/M2GARSS47143.2020.9105197.

[45] Image Processing Research Group (GRIP), “IKONOS imagery”, University Federico II of Naples. [Online]. Available: https://www.grip.unina.it/download/prog/PN